Low-energy quantum gravity and cosmology

Michael A. Ivanov*
Physics Department
Belarus State University of Informatics and Radioelectronics
Minsk, Belarus

Abstract

The model of low-energy quantum gravity by the author is based on the conjecture about the existence of the background of super-strong interacting gravitons, gravity is considered as the screening effect. The Newton constant *G* and the Hubble constant *H* are computable in the model. In this chapter, main effects of the model are discussed, some cosmological consequences are confronted with observations. Galaxy number counts/redshift and counts/magnitude relations are considered. It is shown that this model can fit observations with the theoretical luminosity distance without dark energy. The Hubble parameter of this model is a linear function of the redshift, that is consistent with existing observations. Results of numerical modeling of the influence of the additional deceleration of bodies, and some possibilities to verify the model are described.

PACS : 98.80.Es, 04.50.Kd, 04.60.Bc

1 Introduction

There exist very different approaches to unify general relativity with quantum mechanics or with the standard model of particle physics (SM), but there are almost not theoretical predictions which may be verified by experiments or observations. Known predictions, if the ones are possible, concern mainly Planck-scale physics and geometry, for example, foamy space-time in loop quantum gravity. This poorness of theoretical predictions of existing models and the absence of manifestations of quantum gravity accepted by the scientific community make the situation around quantum gravity very vague: theorists are not sure in the validity of used approaches, experimentalists and observers do not know what to search to help them. Taking into account logical difficulties of existing approaches, the main sought by H. Nicolai [1] about the situation is that we have no other choice but to try to create a future consistent theory out of purely theoretical basics. It seems that one of the possible ways is to choose

some symmetry group which may lead us further as it was by the creation of the SM. But the SM's symmetries were established due to big experimental efforts. From another side, the SM's continuous symmetries may result from underlying discrete symmetries if the fundamental fermions are the two-component composite particles [2, 3]. In any case, even the appearance of the consistent model of quantum gravity talking us about Planck-scale physics cannot help to understand why micro particles prefer not to move along geodesics by small energies which are very far from the Planck scale. Perhaps, we should search and introduce some more non-evident ideas to come nearer to the unknown quantum nature of gravity.

In the model of low-energy quantum gravity [4, 5, 6], gravitation is considered as the screening effect in the sea of super-strong interacting gravitons. The Newton constant G and the Hubble constant H are computable in the model as functions of the background temperature. There is not a need of any expansion of the universe and dark energy in the model to fit corresponding cosmological observations. The two-parametric theoretical luminosity distance of the model is caused by forehead and non-forehead collisions of photons with gravitons. The additional deceleration of massive bodies has the same nature as the redshift of remote objects in the model: these effects are caused by collisions with gravitons, but we should take into account both forehead and backhead collisions with gravitons in a case of massive bodies [7]. Some consequences of the model are described in this chapter.

2 Main features of the model

I would like to describe here some important features of my model of low-energy quantum gravity [4, 5, 6]. It is supposed in it that the background of super-strong interacting gravitons exists with the same temperature T as CMB. In the sea of gravitons, a pressure force of single gravitons and a repulsive force due to scattered gravitons are approximately equal for any pair of usual bodies. But they are three order greater than the Newtonian force between bodies. It leads immediately to the very surprising conclusion: Einstein's equivalence principle would be roughly violated for black holes, because this repulsive force is equal to zero for them. The ratio of gravitational to inertial masses of a black hole is equal to 1215.4. For a binary system of a black hole and a usual body, the third Newtonian law will be broken, too.

If single gravitons of running flux associate in pairs which are destructed in collisions, then we have for the Newton constant G :

$$G \equiv \frac{4}{3} \cdot \frac{D^2 c (kT)^6}{\pi^3 \hbar^3} \cdot I_2, \qquad (1)$$

where $I_2 = 2.3184 \cdot 10^{-6}$. It follows from this expression that by $T = 2.7K$ the new constant D should have the value: $D = 0.795 \cdot 10^{-27} m^2/eV^2$. The inverse-square law of classical gravity describes the main quantum effect of this model. The possibility to calculate G makes the model underlying for general relativity.

To have the condition of big distances: $\sigma(E, <\epsilon>) \quad 4\pi r^2$, where $\sigma(E, <\epsilon>)$ is the cross-section of interaction of gravitons with an average energy $<\epsilon>$ with a particle having an energy E, r is a distance between massive particles, be fulfilled, it is necessary to accept an "atomic structure" of matter, i.e. gravitons cannot interact with big bodies in the aggregate, they may interact only with "small particles" of matter - for example, with atoms.

For photons, there are two small effects in the sea of super-strong interacting gravitons: average energy losses of a photon due to forehead collisions with gravitons and an additional relaxation of a photonic flux due to non-forehead collisions of photons with gravitons. The first effect leads to the geometrical distance/redshift relation:

$$r(z) = ln(1 + z) \cdot c/H_0, \tag{2}$$

where H_0 is the Hubble constant. The both effects lead to the luminosity distance/redshift relation:

$$D_L(z) = c/H_0 \cdot \ln(1 + z) \cdot (1 + z)^{(1+b)/2}, \tag{3}$$

where the "constant" b belongs to the range 0 - 2.137 (b = 2.137 for a very soft radiation, and $b \to 0$ for a very hard one). In the general case it should depend on a rest-frame spectrum and on the redshift. Because of this, the Hubble diagram should be a multivalued function of the redshift: for a given z, b may have different values for different kinds of sources.

The average time delay of photons due to multiple interactions with gravitons of the background is computed in my paper [8]. The two variants of evaluation of the lifetime of a virtual photon are considered: 1) on a basis of the uncertainties relation (it is a common place in physics of particles) and 2) using a conjecture about constancy of the proper lifetime of a virtual photon. In the first case Lorentz violation is negligible: the ratio of the average time delay of photons to their propagation time is equal approximately to 10^{-28}; in the second one (with a new free parameter of the model), the time-lag is proportional to the difference $\sqrt{E_{01}} - \sqrt{E_{02}}$, where E_{01}, E_{02} are initial energies of photons, and more energetic photons should arrive later, also as in the first case. The effect of graviton pairing is taken into account.

The Hubble constant may be computed in the model, too:

$$H_0 = \frac{1}{2\pi} D \cdot \bar{\epsilon} \cdot (\sigma T^4) = (G \frac{45}{64} \frac{\sigma T^4 I_4^2}{c^3 I_2})^{1/2}, \tag{4}$$

where $\bar{\epsilon}$ is an average graviton energy, I_4 = 24.866. We have for its value: $H_0 = 2.14 \cdot 10^{-18}\ s^{-1} = 66.875\ km \cdot s^{-1} \cdot Mpc^{-1}$.

The additional deceleration w of massive bodies has the same nature as the redshift of remote objects in the model: these effects are caused by collisions with gravitons, but we should take into account both forehead and backhead collisions with gravitons in a case of massive bodies [7]. The deceleration w is equal to:

$$w = -w_0 \cdot 4\eta^2 \cdot (1 - \eta^2)^{0.5}, \tag{5}$$

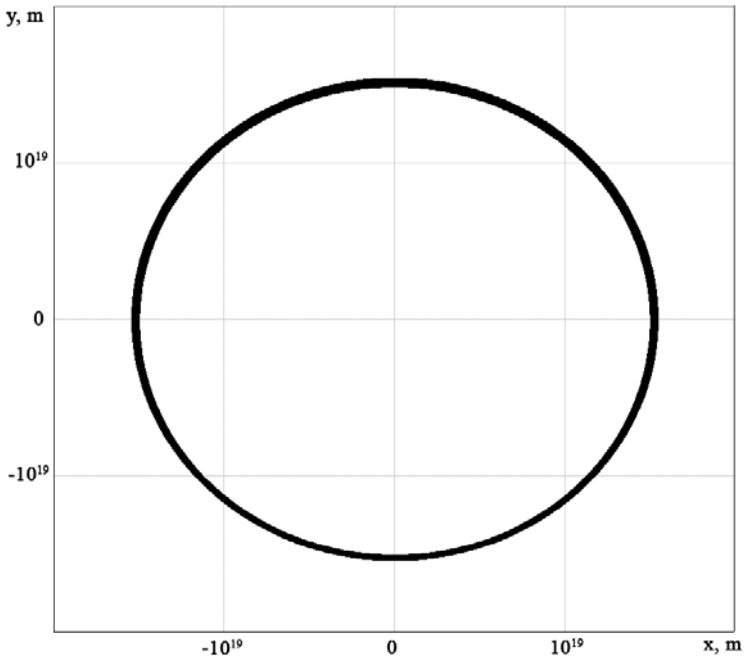

Figure 1: A star orbit in a galaxy with $M = 10^{10} \cdot M_\odot$ by $u = 5 \cdot 10^5$ m/s and $r(0) = 1$ kpc; t 30 Gyr, single loops interflow, the change of the distance to the center $\Delta r/r(0) = -0.034$.

where $w_0 \equiv H_0 c = 6.419 \cdot 10^{-10}$ m/s^2, if we use the theoretical value of H_0 in the model; $\eta \equiv V/c$, V is a body's velocity relative to the graviton background. For small velocities we have:

$$w \quad -w_0 \cdot 4\eta^2. \tag{6}$$

3 Modified dynamics in the graviton background

Some results of numerical modeling of a motion of bodies in the central field by the influence of this additional deceleration are described in this section [10].

In the Newtonian approach, if $\mathbf{u}$ is a more massive body's velocity relative to the background, M is its mass, and $\mathbf{V} = \mathbf{v} + \mathbf{u}$ is the velocity of the small body relative to the graviton background, we will have now the following equation of motion of the small body:

$$\ddot{\mathbf{r}} = -G\frac{M}{r^2} \cdot \frac{\mathbf{r}}{r} + \frac{4w_0}{c^2}(u \cdot \mathbf{u} - |\mathbf{v} + \mathbf{u}| \cdot (\mathbf{v} + \mathbf{u})), \tag{7}$$

where $\mathbf{r}$ is a radius-vector of the small body.

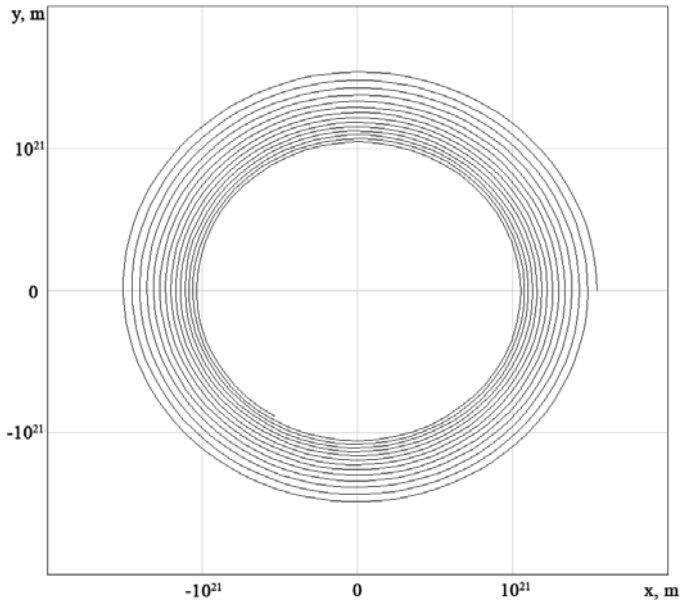

Figure 2: A star orbit in a galaxy with $M = 10^{10}\ M_\odot$ by $u = 5 \cdot 10^5$ m/s and $r(0) = 100$ kpc; t 300 Gyr, the first unclosed external loop corresponds to 29.2 Gyr.

To model the motion in the central field, I have slightly modified the program in C++ written for our work [9] to work in 3 dimensions using Eq. 7.

Let us consider the initial conditions by which a material point trajectory in the classical case is circular, i.e. $v(0) = (G\ M/r(0))^{0.5}$, and $\mathbf{v}(0) \perp \mathbf{r}(0)$, T is a period of motion in the classical case of a circular trajectory by the given initial distance to the center. To evaluate a stability of planetary orbits in the solar system in a presence of the anomalous deceleration w, we can use the following trick: to increase w by hand to see a very small change of the orbit's radius, and to re-calculate a value of the resulting effect. In a case of the Earth-like circular orbit, i.e. by $M = M_\odot$, $r(0) = 1$ AU, given $u = 4 \cdot 10^5$ m/s and that three vectors $\mathbf{r}$, $\mathbf{v}$, $\mathbf{u}$ lie in one plane, we get by the replacement: $w \to 10^4\ w$ for one classical period T : $\Delta r/r(0) = 1.08 \cdot 10^{-8}$ yr^{-1} by $\Delta t = 10^{-10}\ T$. It means that by the anomalous deceleration w we should have now: $\Delta r/r(0) = 1.08 \cdot 10^{-12}$ yr^{-1}. For the case when $\mathbf{u}$ is perpendicular to $\mathbf{r}$, $\mathbf{v}$ we have: $\Delta r/r(0) = 7.2 \cdot 10^{-13}$ yr^{-1}. The Earth orbit will be stable enough to have not contradictions with the estimated age of it in the solar system.

Results of modeling a star orbit in a galaxy in the similar way are shown in Figures 1 and 2 for $M = 10^{10} \cdot M_\odot$, $u = 5 \cdot 10^5$ m/s by $r(0) = 1$ kpc (Fig. 1) and $r(0) = 100$ kpc (Fig. 2). The ratio $\frac{w_0}{r(0)}$ is equal to 2.2 and 0.00022 respectively. By $r(0) = 1$ kpc the relative change of the distance to the center

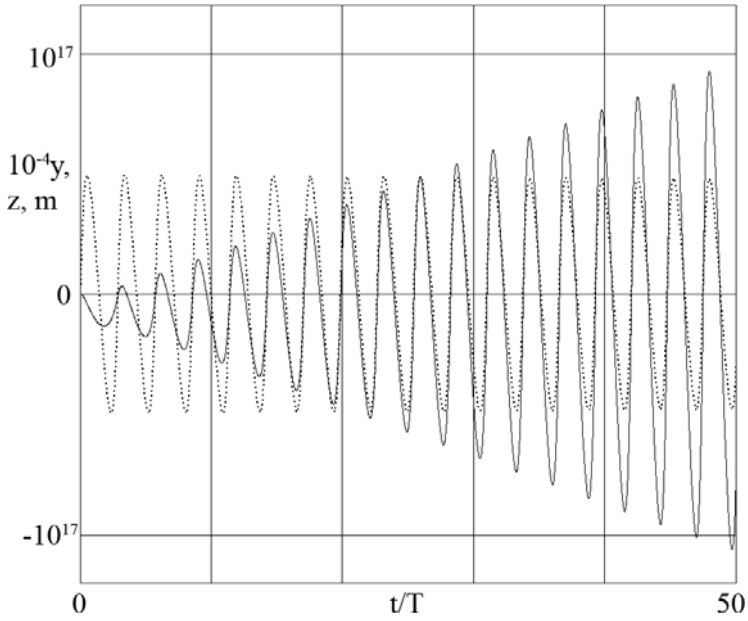

Figure 3: The deviation $z(t)$ (solid) of a star orbit in a galaxy (with $M = 10^{10}\ M_\odot$ by $u = 5\ 10^5$ m/s and $r(0) = 10$ kpc) from the classical plane (x, y) for the case of $v(0) = 1.2\ (G\ M/r(0))^{0.5}$; $T = 0.781$ Gyr, the graph of $10^{-4}\cdot y(t)$ (dotted) is shown for the comparison.

is $\Delta r/r(0) = -0.034$ during the time interval of 30 Gyr. By $r(0) = 1$ kpc the first unclosed external loop in Fig. 2 corresponds to 29.2 Gyr. We see that at all scales closed orbits do not exist in the model: bodies inspiral to the center of attraction, but for the Earth-like orbits this effect is very small.

When **u** is perpendicular to **r**, **v**, another effect takes place: the motion of the body in the central field is not planar. The deviation $z(t)$ of a star orbit in a galaxy (with $M = 10^{10}\ M_\odot$ by $u = 5\ 10^5$ m/s and $r(0) = 10$ kpc) from the classical plane (x, y) is shown in Figures 3 and 4. For the case of $v(0) = (G\ M/r(0))^{0.5}$ (the classical orbit would be circular), deviations from the classical plane (x, y) occur in one side off this plane, with returns to it (Fig. 4). In the case of the Earth-like circular orbit, the maximal deviation from the classical plane is lesser of 1 mm by $u = .4\ 10^5$ m/s. If $v(0) = (G\ M/r(0))^{0.5}$, deviations from the classical plane (x, y) occur in both sides off this plane (Fig. 3, $v(0) = 1.2\ (G\ M/r(0))^{0.5}$), and the ones may be interpreted as a slow revolution of a quasi-classical planar orbit around some axis in this plane.

The described results show two peculiarities of modified dynamics in the model: an absence of closed orbits and a possibility of the non-planar motion of massive bodies in the central field due to the anomalous deceleration by the graviton background. These effects are negligible for the Earth-like orbits

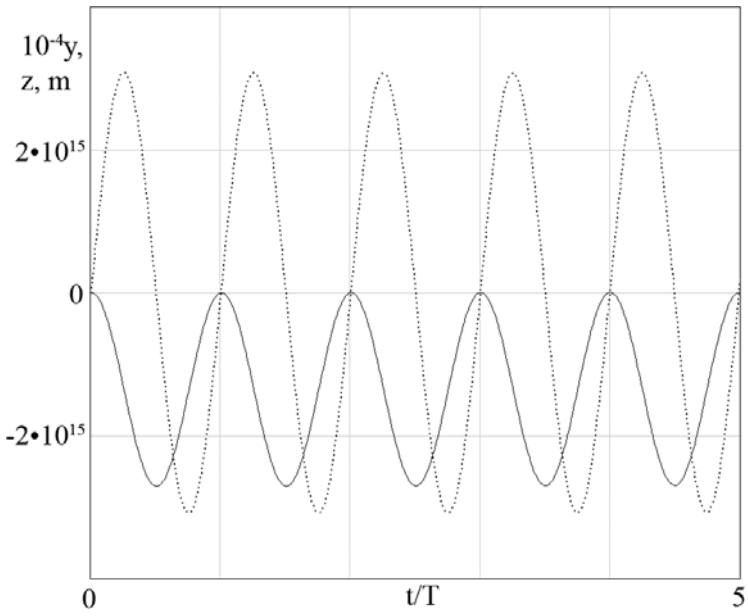

Figure 4: The same graphs as in Fig. 3, but for the case of $v(0) = (G \cdot M/r(0))^{0.5}$; $T = 0.781$ Gyr, $10^{-4} \cdot y$ (dotted), z (solid).

and, perhaps, too small to be observable during an acceptable time interval in galaxies. But the interaction of photons with the background leads to the observable effects which can be essential for our understanding of the universe.

4 Cosmological consequences of the model

Small additional effects of this model have essential cosmological consequences. In the model, redshifts of remote objects and the dimming of supernovae 1a may be interpreted without any expansion of the Universe and without dark energy. Some of these consequences are discussed and confronted with galaxy number counts, supernovae 1a, long GRBs, and QSOs observations in this section. It is shown that the two-parametric theoretical luminosity distance of the model fits observations with high confidence levels, if all data sets are corrected for no time dilation. These two parameters are computable in the model.

4.1 Galaxy number counts

In this subsection, I consider galaxy number counts/redshift and counts/magnitude relations on a basis of this model [11]. I assume here that a space is flat and the Universe is not expanding.

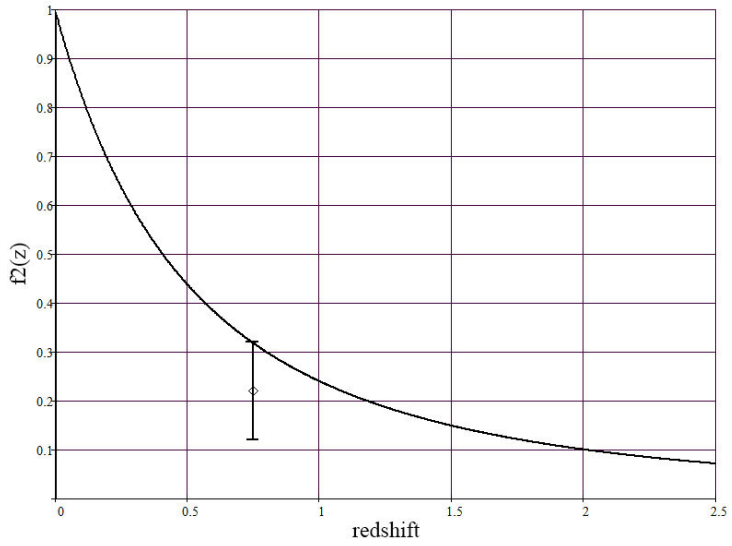

Figure 5: The graph of the function $f_2(z)$ (solid) of this model. The typical error bar and data point are taken from paper by Loh and Spillar [13].

4.1.1 The galaxy number counts-redshift relation

Total galaxy number counts $dN(r)$ for a volume element $dV = d\Omega r^2 dr$ is equal to: $dN(r) = n_g dV = n_g d\Omega r^2 dr$, where n_g is the galaxy number density (it is constant in the no-evolution scenario), $d\Omega$ is a solid angle element. Using the function $r(z)$ of this model, we can re-write galaxy number counts as a function of the redshift z:

$$dN(z) = n_g d\Omega (H_0/c) \; - \frac{ln^2(1+z)}{1+z} dz. \qquad (8)$$

Let us introduce a function (see [12])

$$f_2(z) \equiv \frac{(H_0/c)^3 dN(z)}{n_g d\Omega z^2 dz};$$

then we have for it in this model:

$$f_2(z) = \frac{ln^2(1+z)}{z^2(1+z)}. \qquad (9)$$

A graph of this function is shown in Fig. 5; the typical error bar and data point are added here from paper by Loh and Spillar [13]. There is not a visible contradiction with observations. There is not any free parameter in the model to fit this curve; it is a very rigid case.

It is impossible to count a total galaxy number for big redshifts so as very faint galaxies are not observable. For objects with a fixed luminosity, it is

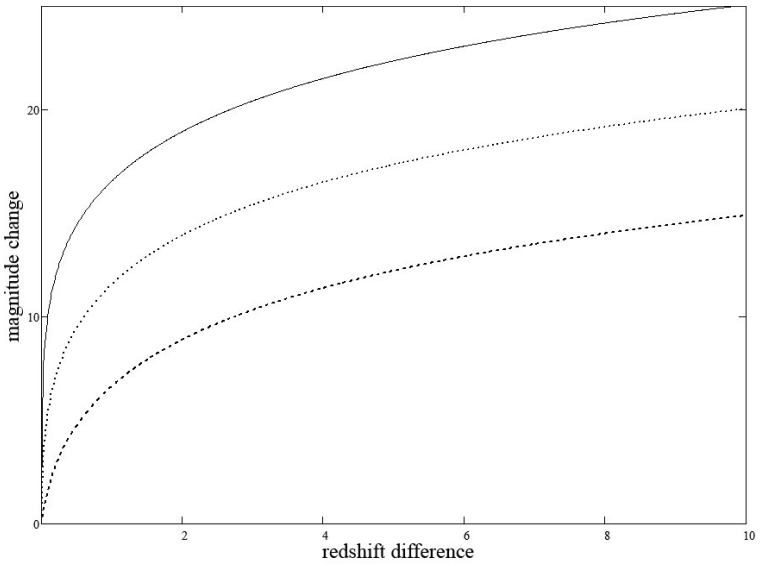

Figure 6: Magnitude changes Δm as a function of the redshift difference $z_2 - z_1$ in this model for $z_1 = 0.001$ (solid); 0.01 (dot); 0.1 (dash).

easy to find how their magnitude m changes with a redshift. So as $dm(z)$ under a constant luminosity is equal to: $dm(z) = 5d(lgD_L(z))$, we have for $\Delta m(z_1, z_2) \equiv \int_{z_1}^{z_2} dm(z)$:

$$\Delta m(z_1, z_2) = 5lg(f_1(z_2)/f_1(z_1)). \qquad (10)$$

The graph of this function is shown in Fig. 6 for $z_1 = 0.001; 0.01; 0.1$.

4.1.2 Taking into account the galaxy luminosity function

Galaxies have different luminosities L, and we can write n_g as an integral: $n_g = \int dn_g(L)$, where $dn_g(L) = \eta(L)dL$, $\eta(L)$ is the galaxy luminosity function. I shall use here the Schechter luminosity function [14]:

$$\eta(L)dL = \varphi_* (\frac{L}{L_*})^{\alpha} exp(-\frac{L}{L_*}) d(\frac{L}{L_*}) \qquad (11)$$

with the parameters φ_*, L_*, α. So as we have by a definition of the luminosity distance $D_L(z)$ that a light flux I is equal to: $I = \frac{L}{4\pi D_L^2(z)}$, and a visible magnitude m of an object is $m = -2.5 \lg I + C$, where C is a constant, then m is equal to:

$$m = -2.5 \lg I + 5 \lg D_L(z) + (C - 4\pi). \qquad (12)$$

We can write for L :

$$L = A \cdot \frac{D_L^2(z)}{K^m}, \qquad (13)$$

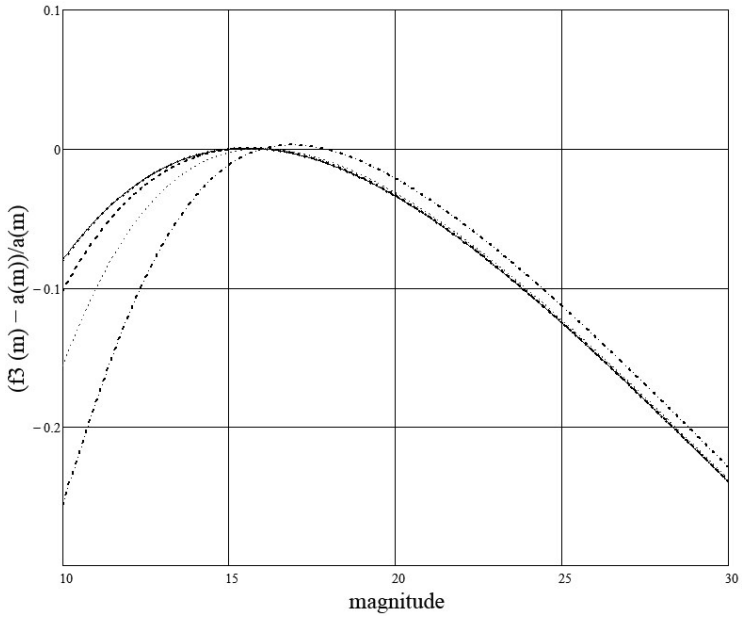

Figure 7: The relative difference $(f_3(m)-a(m))/a(m)$ as a function of the magnitude m for $\alpha = -2.43$ by $10^{-2} < A_1 < 10^2$ (solid), $A_1 = 10^4$ (dash), $A_1 = 10^5$ (dot), $A_1 = 10^6$ (dadot).

where $\kappa = 10^{0.4}$, $A = const.$ For a thin layer with $z = const$ we have:

$$dL = \frac{\partial L}{\partial m} \cdot dm,$$

where

$$\frac{\partial L}{\partial m} = -m\kappa \cdot A \frac{D_L^2(z)}{\kappa^m} = -m\kappa L. \qquad (14)$$

Then

$$dn_g(m,z) = -(\varphi_* \kappa) \cdot I^\alpha(m,z) \exp(-I(m,z)) \cdot (m \cdot I(m,z)) dm, \qquad (15)$$

where $(-dm)$ corresponds to decreasing m by growing L when $z = const$, and

$$I(m,z) \equiv \frac{L(m,z)}{L_*}.$$

Let us introduce a function $f_3(m,z)$ with a differential

$$df_3(m,z) \equiv \frac{dN(m,z)}{d\Omega(-dm).} \qquad (16)$$

We have for this differential in the model:

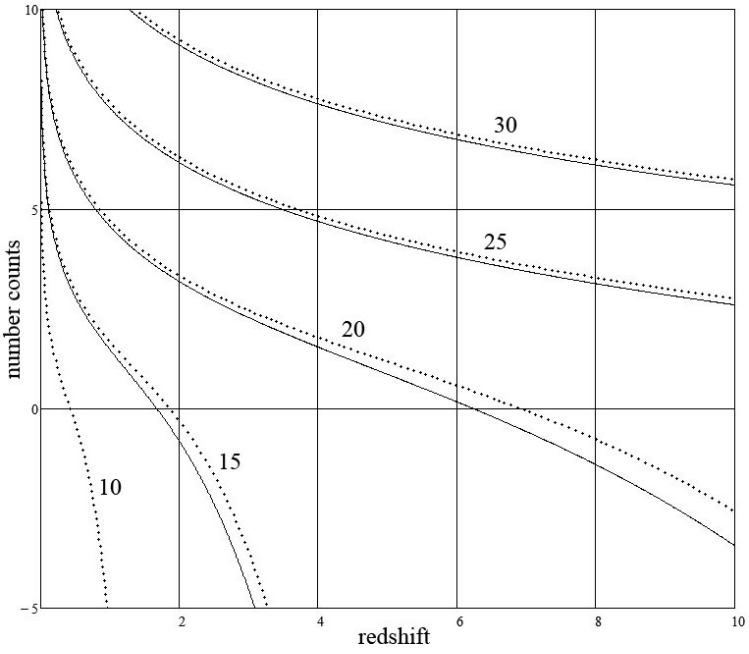

Figure 8: Number counts $f_4(m,\ z)$ (dot) and $f_5(m_1,\ m_2)$ (solid) (logarithmic scale) as a function of the redshift by $A_1 = 10^5$ for $\alpha = -2.43$, $m_1 = 10$ and different values of $m = m_2$: 15, 20, 25, 30; $m = 10$ (only $f_4(m, z)$).

$$df_3(m, z) = \left(\frac{\varphi_* K}{a^3}\right) \cdot m \cdot l^{\alpha+1}(m, z) \cdot \exp(-l(m, z)) \cdot \frac{ln^2(1+z)}{(1+z)} dz, \qquad (17)$$

where $a = H_0/c$. An integral on z gives the galaxy number counts/magnitude relation:

$$f_3(m) = \left(\frac{\varphi_* K}{a^3}\right) \cdot m \cdot \int_0^{z_{max}} l^{\alpha+1}(m, z) \cdot \exp(-l(m, z)) \cdot \frac{ln^2(1+z)}{(1+z)} dz; \qquad (18)$$

I use here an upper limit $z_{max} = 10$. To compare this function with observations by Yasuda et al. [15], let us choose the normalizing factor from the condition: $f_3(16) = a(16)$, where

$$a(m) \equiv A_\lambda \cdot 10^{0.6(m-16)} \qquad (19)$$

is the function assuming "Euclidean" geometry and giving the best fit to observations [15], $A_\lambda = const$ depends on the spectral band. In this case, we have two free parameters - α and L_* - to fit observations, and the latter one is connected with a constant $A_1 \equiv \frac{A}{a^2 L_*}$ if

$$l(m, z) = A_1 \frac{f_1^2(\ )}{K^m}.$$

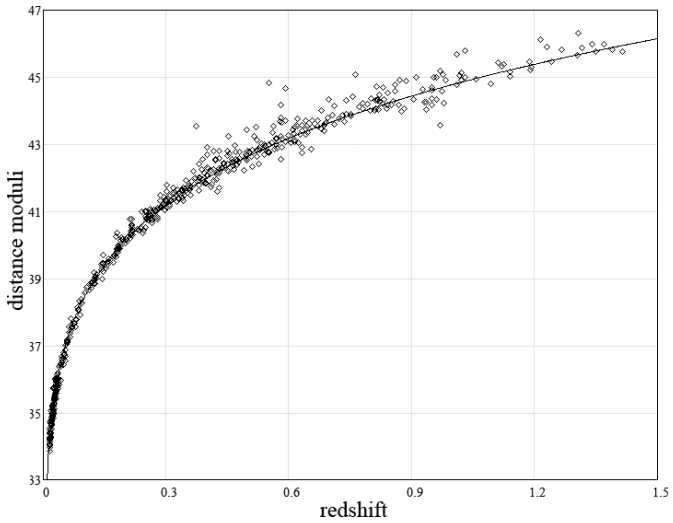

Figure 9: The theoretical Hubble diagram $\mu_0(z)$ of this model (solid); Supernovae 1a observational data (580 points of the SCP Union 2.1 compilation) are taken from [18] and corrected for no time dilation.

If we use the magnitude scale in which $m = 0$ for Vega then $C = 2.5 \lg I_{Vega}$, and we get for A_1 by $H_0 = 2.14 \cdot 10^{-18} s^{-1}$ (it is a theoretical estimate of H_0 in this model):

$$A_1 \quad 5 \cdot 10^{17} \cdot \frac{L_\odot}{L}, \tag{20}$$

where $L_\odot$ is the Sun luminosity; the following values are used: $L_{Vega} = 50 L_\odot$, the distance to Vega $r_{Vega} = 26$ *LY*.

Without the factor m, the function $f_3(m)$ by $\exp(-l(m, z) \rightarrow 1$ would be close to $a(m)$ by $\alpha = -2.5$. Matching values of α shows that $f_3(m)$ is the closest to $a(m)$ in the range $10 < m < 20$ by $\alpha = -2.43$. The ratio $\frac{f_3(m)-a(m)}{a(m)}$ is shown in Fig. 7 for different values of A_1 by this value of α (to turn aside the problem with divergencies of this function by small L for negative values of α, all computations are performed here for $z > 0.001$). All such the curves conflow by $A_1 \leq 10^2$ (or $5\ 10^{15} < L_*$), i.e. observations of the galaxy number counts/magnitude relation are non-sensitive to A_1 in this range. For fainter magnitudes $20 < m < 30$, the behavior of all curves is identical: they go below of the ratio value 1 with the same slope. If we compare this figure with Figs. 6,10,12 from [15], we see that the considered model provides a no-worse fit to observations than the function $a(m)$ if the same K-corrections are added (perhaps, even the better one if one takes into account positions of observational points in Figs. 6,10,12 from [15] by $m < 16$ and $m > 16$) for the range $10^2 < A_1 < 10^7$ that corresponds to $5 \cdot 10^{15} > L_* > 5 \cdot 10^{10}$.

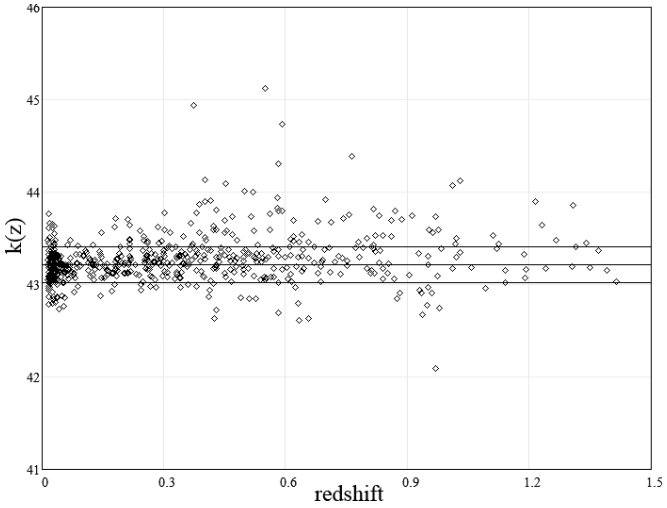

Figure 10: Values of $k(z)$ (580 points) and $< k(z) >$, $< k(z) > +\sigma_k$, $< k(z) > -\sigma_k$ (lines) for the SCP Union 2.1 compilation.

Observations of $N(z)$ for different magnitudes are a lot more informative. If we define a function $f_4(m, z)$ as

$$f_4(m, z) \equiv \left(\frac{a^3}{\varphi_k}\right) \cdot \frac{df_3(m, z)}{dz}, \tag{21}$$

this function is equal in the model to:

$$f_4(m, z) = m \cdot l^{\alpha+1}(m, z) \cdot \exp(-l(m, z)) \cdot \frac{ln^2(1 + z)}{(1 + z)}. \tag{22}$$

Galaxy number counts in the range $m_1 < m < m_2$ are proportional to the function:

$$f_5(m_1, m_2) \equiv \int_{m_1}^{m_2} f_4(m, z)dm = \tag{23}$$

$$= \int_{m_1}^{m_2} m \cdot l^{\alpha+1}(m, z) \cdot \exp(-l(m, z)) \cdot \frac{ln^2(1 + z)}{(1 + z)}dm.$$

Graphs of both $f_4(m, z)$ and $f_5(m_1, m_2)$ are shown in Fig. 8 by $\alpha = 2.43$, $A_1 = 10^5$; they are very similar between themselves. We see that even the observational fact that a number of visible galaxies by $z \sim 10$ is very small allows us to restrict a value of the parameter A_1 much stronger than observations of $N(m)$. Quasar number counts are considered in [11], too.

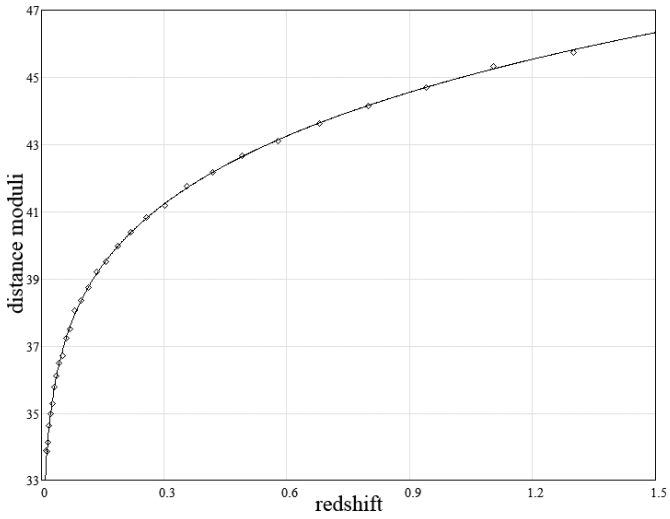

Figure 11: The theoretical Hubble diagram $\mu_0(z)$ of this model with $b = 2.365$ (solid); Supernovae 1a observational data (31 binned points of the JLA compilation) are taken from Tables F.1 and F.2 of [19] and corrected for no time dilation.

4.2 Fitting observations with the theoretical luminosity distance

4.2.1 The Hubble diagram of this model

In this model, the luminosity distance is given by *Eq.* 3. The theoretical value of relaxation factor b for a soft radiation is $b = 2.137$. Let us begin with this value of b, considering the Hubble constant as a single free parameter to fit observations [16]. All observational data should be corrected for no time dilation as: $\mu(z)$ $\mu(z) + 2.5\ lg(1+z)$ in this model without expansion.

Two big compilations of SN 1a observations are used here: the SCP Union 2.1 compilation (580 supernovae) [18] and the JLA compilation (740 supernovae) [19]. These compilations may be used to evaluate the Hubble constant in this approach. Using the definition of distance modulus: $\mu(z) = 5lgD_L(z)(Mpc) + 25$, we get from *Eq.* 3 for the theoretical distance modulus $\mu_0(z)$: $\mu_0(z) = 5lgf_1(z) + k$, where $f_1(z) \equiv \ln(1+z) \cdot (1+z)^{(1+b)/2}$, and the constant k is equal to:

$$k \equiv 5lg(c/H_0) + 25.$$

If the model fits observations, then we shall have for $k(z)$:

$$k(z) = \mu(z) - 5lgf_1(z), \tag{24}$$

where $\mu(z)$ is an observational value of distance modulus. The weighted average

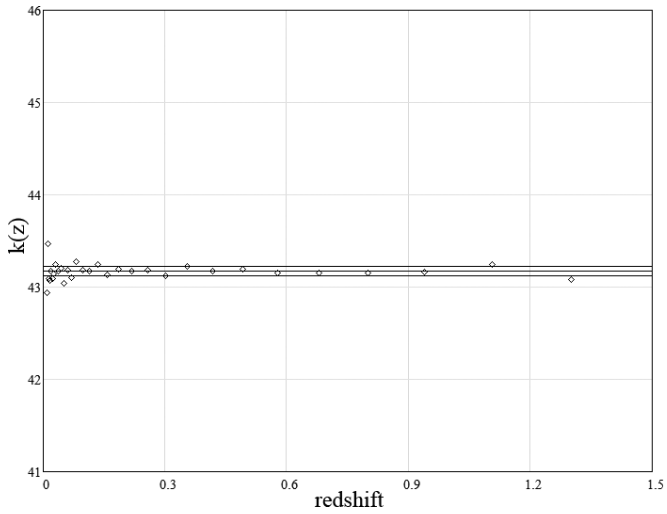

Figure 12: Values of $k(z)$ (31 binned points) and $< k(z) >$, $< k(z) > +\sigma_k$, $< k(z) > -\sigma_k$ (lines) for the JLA compilation.

value of $k(z)$:

$$< k(z) > = \sum_i k(z_i)/\sigma_i^2, \qquad (25)$$

where σ_i^2 is a dispersion of $\mu(z_i)$, will be the best estimate of k. Here, σ_i^2 is defined as: $\sigma_i^2 = \sigma_{i\,stat}^2 + \sigma_{i\,sys}^2$. The average value of the Hubble constant may be found as:

$$< H_0 >= \frac{c \cdot 10^5}{10^{<k(z)>/5} \cdot Mpc}. \qquad (26)$$

For a standard deviation of the Hubble constant we have:

$$\sigma_0 = \frac{ln10 \cdot < H_0 >}{5} \cdot \sigma_k, \qquad (27)$$

where σ_k^2 is a weighted dispersion of k, which is calculated with the same weights as $< k(z) >$.

The theoretical Hubble diagram $\mu_0(z)$ of this model with $< k(z) >$ which is calculated using the SCP Union 2.1 compilation [18] is shown in Fig. 9 together with observational points corrected for no time dilation. Values of $k(z)$ (580 points) and $< k(z) >$, $< k(z) > +\sigma_k$, $< k(z) > \sigma_k$ (lines) are shown in Fig. 10. For this compilation we have: $< k > \pm\sigma_k = 43.216 \pm 0.194$. Calculating the χ^2 value as:

$$\chi^2 = \sum \frac{(k(z_i) - < H_0 >)^2}{\sigma_i^2}, \qquad (28)$$

we get $\chi^2 = 239.635$. By 579 degrees of freedom of this data set, it means that the hypothesis that $k(z) = const$ cannot be rejected with 100% C.L. Using

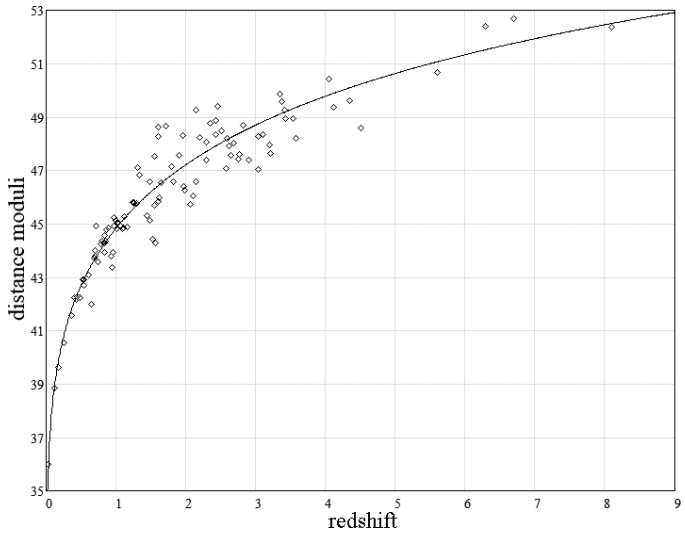

Figure 13: The theoretical Hubble diagram $\mu_0(z)$ of this model (solid); long GRBs observational data (109 points) are taken from Tables 1,2 of [20] and corrected for no time dilation.

Eqs. 25, 26, we get for the Hubble constant from the fitting:

$$< H_0 > \pm\sigma_0 = (2.211 \pm 0.198) \cdot 10^{-18}\ s^{-1} = (68.223 \pm 6.097)\frac{km}{s \cdot Mpc}.$$

The theoretical value of the Hubble constant in the model: $H_0 = 2.14\ 10^{-18}\ s^{-1} = 66.875\ km \cdot s^{-1} \cdot Mpc^{-1}$ belongs to this range. The traditional dimension $km\ s^{-1}\ Mpc^{-1}$ is not connected here with any expansion.

To repeat the above calculations for the JLA compilation, I have used 31 binned points from Tables F.1 and F.2 of [19] (diagonal elements of the correlation matrix in Table F.2 are dispersions of distance moduli). We have for this compilation by $b = 2.137$: $< k > \pm\sigma_k = 43.174 \pm 0.049$ with $\chi^2 = 51.66$. By 30 degrees of freedom of this data set, it means that the hypothesis that $k(z) = const$ cannot be rejected only with 0.83% C.L. Varying the value of b, we find the best fitting value of this parameter: $b = 2.365$ with $\chi^2 = 30.71$. It means that the hypothesis that $k(z) = const$ cannot be rejected now with 43.03% C.L. This value of b is 1.107 times greater than the theoretical one. For the Hubble constant we have in this case:

$$< H_0 > \pm\sigma_0 = (2.254 \pm 0.051) \cdot 10^{-18}\ s^{-1} = (69.54 \pm 1.58)\frac{km}{s \cdot Mpc}.$$

Results of the best fitting are shown in Figs. 11,12.

If observations of long Gamma-Ray Bursts (GRBs) for small z are calibrated using SNe 1a, observational points are fitted with this theoretical Hubble diagram, too [6]. But for hard radiation of GRBs, the factor b may be smaller,

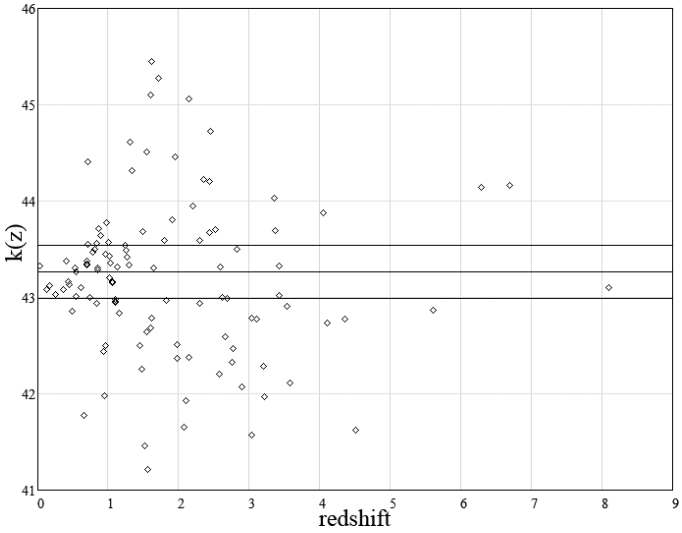

Figure 14: Values of $k(z)$ (109 points) and $< k(z) >$, $< k(z) > +\sigma_k$, $< k(z) > -\sigma_k$ (lines) for long GRBs.

and the real diagram for them may differ from the one for SNe 1a. With this limitation, the long GRBs observational data (109 points) are taken from Tables 1,2 of [20] and fitted in the same manner with $b = 2.137$. In this case we have: $< k > \pm\sigma_k = 43.262 \pm 8.447$ with $\chi^2 = 70.39$. By 108 degrees of freedom of this data set, it means that the hypothesis that $k(z) = const$ cannot be rejected with 99.81% C.L. For the Hubble constant we have in this case:

$$< H_0 > \pm\sigma_0 = (2.162 \pm 0.274) \cdot 10^{-18}\ s^{-1} = (66.71 \pm 8.45)\frac{km}{s \cdot Mpc}.$$

Results of the fitting are shown in Figs. 13,14.

A data set of 44 long Gamma-Ray Bursts was compiled with the redshift range of [0.347; 9.4] [21], in which two empirical luminosity correlations (the Amati relation and Yonetoku relation) were used to calibrate observations. Because the GRB Hubble diagram calibrated using luminosity correlations is almost independent on the GRB spectra, as it has been shown by the authors, I use here values of $\mu(z_i) \pm \sigma_i$ from columns 7 of Tables 2 and 3 of [21], based on the Band function, but with both calibrations. If this data set is fitted in the same manner with $b = 2.137$, we have for the Amati calibration: $< k > \pm \sigma_k = 43.168 \pm 1.159$ with $\chi^2 = 40.585$. By 43 degrees of freedom of this data set, it means that the hypothesis that $k(z) = const$ cannot be rejected with 57.66% C.L. For the Hubble constant we have in this case:

$$< H_0 > \pm\sigma_0 = (2.26 \pm 1.206) \cdot 10^{-18}\ s^{-1} = (69.732 \pm 37.226)\frac{km}{s \cdot Mpc}.$$

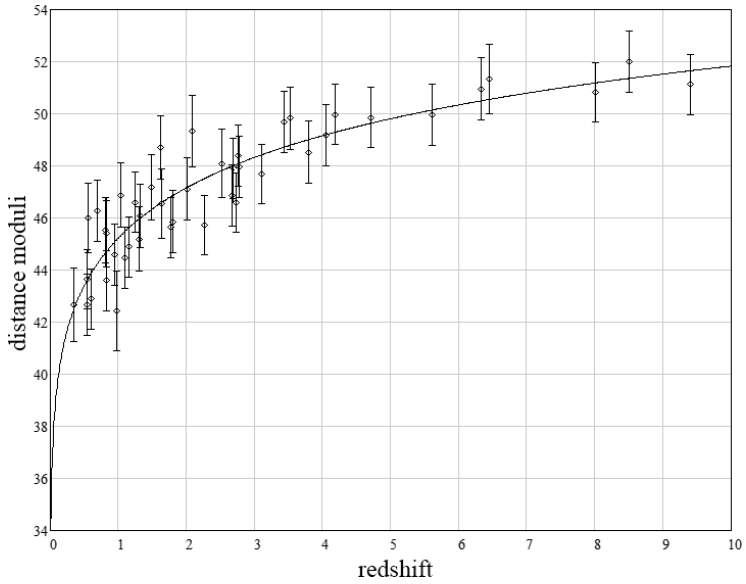

Figure 15: The theoretical Hubble diagram $\mu_0(z)$ of this model with b = 1.11 (solid); GRB observational data with the Yonetoku calibration (44 points) are taken from Table 3 of [21] and corrected for no time dilation.

By b = 2.137, we have for the Yonetoku calibration: $< k > \pm \sigma_k = 43.148 \pm 1.197$ with $\chi^2 = 43.148$. It means that the hypothesis that $k(z) = const$ cannot be rejected with 46.5% C.L. For the Hubble constant we have in this case:

$$< H_0 > \pm \sigma_0 = (2.281 \pm 1.257) \cdot 10^{-18}\ s^{-1} = (70.386 \pm 38.793)\frac{km}{s \cdot Mpc}.$$

But best fitting values of b are less than 2.137 in both cases: b = 1.885 for the Amati calibration ($< k > \pm \sigma_k = 43.484 \pm 1.15$, $\chi^2 = 39.92$, with 60.57% C.L. and $< H_0 > \pm \sigma_0 = (1.954 \pm 1.035) \cdot 10^{-18}\ s^{-1} = (60.309 \pm 31.932)$*km/s/Mpc.*), and b = 1.11 for the Yonetoku one ($< k > \pm \sigma_k = 44.439 \pm 1.037$, $\chi^2 = 32.58$, with 87.62% C.L. and $< H_0 > \pm \sigma_0 = (1.259 \pm 0.601) \cdot 10^{-18}\ s^{-1} = (38.841 \pm 18.546)$*km/s/M pc.*). Namely smaller values of this parameter for bigger photon energies are expected in the model. For best fitting values of b, values of distance moduli are overestimated in both calibrations: on ~ 0.225 for the Amati calibration, and on ~ 1.18 for the Yonetoku calibration, if we compare values of $< k >$ with its theoretical value of 43.259. It leads to the corresponding underestimation of the Hubble constant. Results of the best fitting for the Yonetoku calibration are shown in Fig. 15.

A new method to test cosmological models was introduced, based on the Hubble diagram for quasars [22]. The authors built a data set of 1,138 quasars for this purpose. Some later, this method and the data set were used to compare

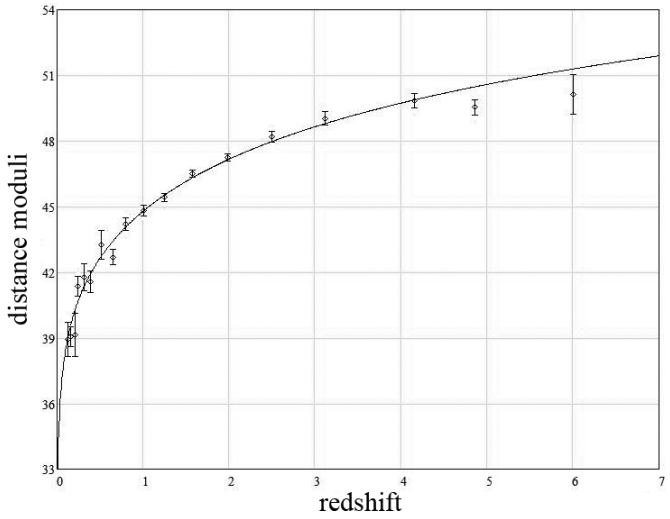

Figure 16: The theoretical Hubble diagram $\mu_0(z)$ of this model (solid); quasar observational data (18 binned points) [23] are corrected for no time dilation.

different models [23]. I have used here the binned quasar data set (18 binned points) of the paper [23] to verify my model in the described above manner. This data set contains the sum of observed distance modulus and an arbitrary constant A. To find this unknown constant for the calibration of QSO observations, I have computed $< k'(z) >=< k(z) > +A$ and replaced $< k(z) >$ by its value for the JLA compilation; it gave: $A = 50.248$. This linking means that the average values of the Hubble constant should be identical for the two data sets. Subtracting this value of A, we get from the fitting of the quasar data by $b = 2.137$: $< k > \pm\sigma_k = 43.175 \pm 0.340$ with $\chi^2 = 23.378$. By 17 degrees of freedom of this data set, it means that the hypothesis that $k(z) = const$ cannot be rejected now with 13.73% C.L. For the Hubble constant we have:

$$< H_0 > \pm\sigma_0 = (2.253 \pm 0.340) \cdot 10^{-18}\ s^{-1} = (69.534 \pm 10.873)\frac{km}{s \cdot Mpc}.$$

Results of the fitting are shown in Fig. 16.

4.2.2 Comparison with the *LCDM* cosmological model

The luminosity distance in the concordance cosmology by $w = -1$ is:

$$D_L(z) = c/H_0 \cdot (1+z) \int_0^z [(1+x)^3\Omega_M + (1-\Omega_M)]^{-0.5} dx \equiv c/H_0 \cdot f_2(z), \quad (29)$$

where $f_2(z) \equiv (1+z)\int_0^z [(1+x)^3\Omega_M + (1-\Omega_M)]^{-0.5}$, Ω_M is the normalized matter density. To compare the above results of fitting with results for the

LCDM cosmology, let us replace $f_1(z) \rightarrow f_2(z)$ and repeat the calculations. Of course, all data sets should remain now corrected for time dilation. The results of fitting are presented in Table 1; for convenience, the main above results for the model of low-energy quantum gravity are collected in the table, too. It is obvious, that confidence levels for both models do not allow to reject any of them.

the model of low-energy quantum gravity				
Data set	b	χ^2	C.L., %	$< H_0 > \pm\sigma_0$
SCP Union 2.1 [18]	2.137	239.635	100	68.22 ± 6.10
JLA [19]	2.365	30.71	43.03	69.54 ± 1.58
109 long GRBs [20]	2.137	70.39	99.81	66.71 ± 8.45
44 long GRBs [21],	2.137	40.585	57.66	69.73 ± 37.23
the Amati calibration	**1.885**	39.92	60.57	60.31 ± 31.93
44 long GRBs [21],	2.137	43.148	46.5	70.39 ± 38.79
the Yonetoku calibration	**1.11**	32.58	87.62	38.84 ± 18.55
quasars [23]	2.137	23.378	13.73	69.53 ± 10.87
the *LCDM* cosmological model				
Data set	Ω_M	χ^2	C.L., %	$< H_0 > \pm\sigma_0$
SCP Union 2.1 [18]	0.30	217.954	100	69.68 ± 5.94
JLA [19]	0.30	29.548	48.90	70.08 ± 1.56
109 long GRBs [20]	0.30	66.457	99.94	70.04 ± 8.62
44 long GRBs [21],	0.30	40.777	56.81	68.99 ± 36.92
the Amati calibration	**0.49**	40.596	57.61	60.75 ± 32.44
44 long GRBs [21],	0.30	38.456	66.85	69.59 ± 36.10
the Yonetoku calibration	**1.0**	34.556	81.72	49.51 ± 24.35
quasars [23]	0.30	21.368	21.03	69.68 ± 10.42

Table 1: Results of fitting the Hubble diagram with the model of low-energy quantum gravity and the *LCDM* cosmological model. The best fitting values of b and Ω_M for 44 long GRBs are marked by the bold typeface.

It is a big surprise that the Einstein–de Sitter model (*Eq.* 29 with $\Omega_M = 1$) cannot be rejected on a base of the full SCP Union 2.1 data set and the χ^2 -criterion. We get $\chi^2 = 428.579$ and 99.9999% C.L. The cause is in a big number of small-z supernovae 1a in this set; it leads to a big number of degrees of freedom, but to small differences of χ^2 for models with similar values of $D_L(z)$ in this range of z. But if one splits the data set in two subsets, for example with $z \leq 0.5$ and $z > 0.5$, and uses the first subset to evaluate $< H_0 >$, then using this $< H_0 >$ and the second subset to compute χ^2 by much smaller number of degrees of freedom, one can reject this model with high probability (when $z > 0.5$, we get $\chi^2 = 247.551$ by 166 observations and 0.004% C.L.). Results for the model of low-energy quantum gravity and the *LCDM* cosmological model are not essentially changed by the splitting. But the Einstein–de Sitter model with $\Omega_M = 1$ bests the *LCDM* cosmological model with any amount of dark

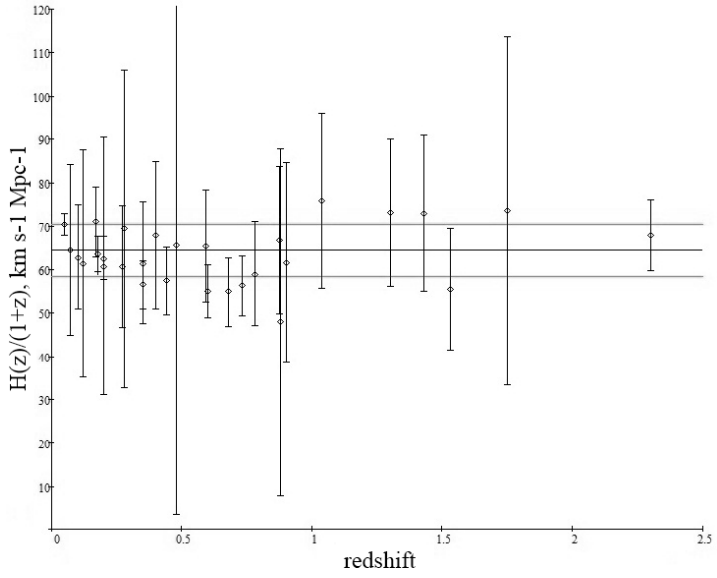

Figure 17: The ratio $H(z)/(1+z)$ $\pm\sigma$ and the weighted value of the Hubble constant $< H_0 >$ $\pm\sigma_{H_0}$ (horizontal lines). Observed values of the Hubble parameter $H(z)$ are taken from Table 1 of [24] and one point for $z < 0.1$ is taken from [25].

energy for the 44 long GRBs data set with the Yonetoku calibration.

4.3 The Hubble parameter of this model

If the geometrical distance is described by *Eq.* 2, for a remote region of the universe we may introduce the Hubble parameter $H(z)$ in the following manner:

$$dz = H(z) \cdot \frac{dr}{c}, \tag{30}$$

to imitate the local Hubble law. Taking a derivative $\frac{dr}{dz}$ we get in this model for $H(z)$:

$$H(z) = H_0 \cdot (1 + z). \tag{31}$$

It means that in the model:

$$\frac{H(z)}{(1+z)} = H_0. \tag{32}$$

The last formula gives us a possibility to evaluate the Hubble constant using observed values of the Hubble parameter $H(z)$. To do it, I use here 28 points of $H(z)$ from [24] and one point for $z < 0.1$ from [25]. The last point is the result

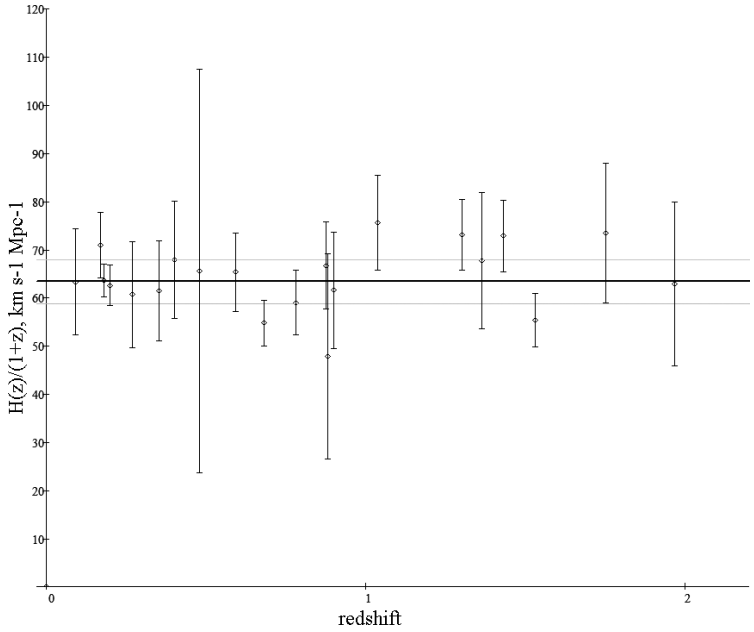

Figure 18: The ratio $H(z)/(1+z)$ $\pm\sigma$ and the weighted value of the Hubble constant $< H_0 >$ $\pm\sigma_0$ (horizontal lines). Observed values of the Hubble parameter $H(z)$ are taken from [26].

of HST measurement of the Hubble constant obtained from observations of 256 low-z supernovae 1a. Here I refer this point to the average redshift $z = 0.05$. Observed values of the ratio $H(z)/(1+z)$ with $\pm\sigma$ error bars are shown in Fig. 17 (points). The weighted average value of the Hubble constant is calculated by the formula:

$$< H_0 >= \frac{\sum \frac{H(z_i)}{1+z_i}/\sigma_i^2}{\sum 1/\sigma_i^2}. \qquad (33)$$

The weighted dispersion of the Hubble constant is found with the same weights:

$$\sigma_0^2 = \frac{\sum (\frac{H(z_i)}{1+z_i} - < H >)^2/\sigma_i^2}{\sum 1/\sigma_i^2}. \qquad (34)$$

Calculations give for these quantities:

$$< H_0 > \pm\sigma_0 = (64.40 \pm 5.95)\ km\ s^{-1}\ Mpc^{-1}. \qquad (35)$$

The weighted average value of the Hubble constant with $\pm\sigma_0$ error bars are shown in Fig. 17 as horizontal lines.

Calculating the χ^2 value as:

$$\chi^2 = \sum \frac{(\frac{H(z_i)}{1+z_i} - < H_0 >)^2}{\sigma_i^2}, \qquad (36)$$

we get $\chi^2 = 16.491$. By 28 degrees of freedom of our data set, it means that the hypothesis described by *Eq.* 31 cannot be rejected with 95% C.L.

If we use another set of 21 cosmological model-independent measurements of H(z) based on the differential age method [26], we get (see Fig. 18):

$$< H_0 > \pm \sigma_0 = (63.37 \pm 4.56)\ km\ s^{-1}\ Mpc^{-1}. \qquad (37)$$

The value of χ^2 in this case is smaller and equal to 3.948. By 21 degrees of freedom of this new data set, it means that the hypothesis described by *Eq.* 31 cannot be rejected with 99.998% C.L.

Some authors try in a frame of models of expanding universe to find deceleration-acceleration transition redshifts using the same data set (for example, [24]). The above conclusion that the ratio $H(z)/(1 + z)$ remains statistically constant in the available range of redshifts is model-independent. For the considered model, it is an additional fact against dark energy as an admissible alternative to the graviton background.

4.4 The Alcock-Paczynski test of the model

The Alcock-Paczynski cosmological test consists in an evaluation of the ratio of observed angular size to radial/redshift size [27]. This test has been carried out for a few cosmological models by Fulvio Melia and Martin Lopez-Corredoira [28]. They used model-independent data on BAO peak positions from [29] and [30]. For two mean values of z ($< z >= 0.57$ and $< z >= 2.34$), the measured angular-diameter distance $d_A(z)$ and Hubble parameter $H(z)$ give for the observed characteristic ratio $y_{obs}(z)$ of this test the values: $y_{obs}(0.57) = 1.264 \pm 0.056$ and $y_{obs}(2.34) = 1.706 \pm 0.076$. In this model we have: $d_{com}(z) = d_A(z) = r(z)$, where $d_{com}(z)$ is the cosmological comoving distance. Because the Universe is static here, the ratio $y(z)$ for this model is defined as:

$$y(z) = \frac{r(z)}{z \cdot \frac{d}{dz} r(z)} = \frac{r(z) \cdot H(z)}{cz} = (1 + \frac{1}{z}) \cdot \ln(1 + z), \qquad (38)$$

where $H(z)$ is defined by *Eq.* 31. This function without free parameters characterizes any tired light model (model 6 in [28]). We have only two observational points to fit them with this function. Calculating the χ^2 value as:

$$\chi^2 = \sum \frac{(y_{obs}(z_i) - y(z_i))^2}{\sigma_i^2}, \qquad (39)$$

we get $\chi^2 = 0.189$, that corresponds to the confidence level of 91% for two degrees of freedom.

5 The light-from-nowhere effect

The additional relaxation of a photonic flux of a remote galaxy due to non-forehead collisions of photons with gravitons is accompanied with the deviation of some part of photons from the galaxy-observer direction. Given multiple collisions on their long ways, the number of initial photons scattered in such the manner rises quickly, and each of them may be scattered again and again. It should lead to the appearance of a diffuse background with a complex spectrum. A tentative detection of a diffuse cosmic optical background [33] may be connected with this light-from-nowhere effect.

To evaluate how big is the ratio $\delta(z)$ of the scattered flux to the the remainder $\Phi(z) \equiv L/D_L^2(b, z)$ reaching the observer, we can compute the flux $\Phi_0(z) \equiv L/D_L^2(0, z)$, where L is the luminosity, $D_L(b, z)$ and $D_L(0, z)$ are luminosity distances by $b = 0$ and $b = 0$. $\Phi_0(z)$ corresponds to the absence of non-forehead collisions. Then the ratio may be defined as:

$$\delta(z) \equiv (\Phi(z) - \Phi_0(z))/\Phi(z). \tag{40}$$

Using *Eq.* 3 we get:

$$\delta(z) = (1 + z)^b - 1. \tag{41}$$

We have by $b = 2.137$: $\delta(1) = 3.34$, $\delta(2) = 9.46$, $\delta(10) = 167.06$. To find the sky brightness in the optical range, for example, it is necessary to know the ratio $\delta(z)$, and, at least, the light flux of galaxies and their number counts by different redshifts.

6 Conclusion

The Newton constant G has been measured up to now with the relative standard uncertainty only $\sim 10^{-4}$ (about the long story of these measurements, see [31]). In the model, the Newton constant arises as an average value of the stochastic variable characterizing the interaction of a couple of bodies with a huge number of gravitons. Uncertainties of G and T are connected as:

$$\frac{\Delta G}{G} = 6\frac{\Delta T}{T}.$$

If fluctuations of the temperature of the graviton background have the same order of magnitude as the ones of the CMB temperature, then $\Delta G/G \leq 6\ 10^{-4}$. It is important that measured values of G may depend on the orientation of two bodies relatively of remote stars. Further attempts to measure G taking into account these circumstances may be interesting for the verification.

In this model, the luminosity distance is a multivalued function of the redshift due to different values of the factor b for soft and hard radiation. It opens another way to verify the model by cosmological observations comparing the Hubble diagrams of sources with different spectra. But to realize it we should have the possibility to calibrate the luminosity, for example, of remote GRBs independently of the Hubble diagram of supernovae Ia.

The Hubble parameter $H(z)$ of this model is a linear function of z: $H(z) = H_0 \cdot (1 + z)$ (as well as in the $R_h = ct$ cosmological model [32]), that is in a big discrepancy with ΛCDM. As it was shown, this function fits available observations of $H(z)$ very well [6, 32], and further investigations of this problem are important.

The most important cosmological consequence of the model is the local quantum nature of redshifts of remote objects. At present, advanced *LIGO* technologies may be partly used to verify this redshift mechanism in a ground-based laser experiment [6]. One should compare spectra of laser radiation before and after passing some big distance in a high-vacuum tube. If one constructs a future version of the *LIGO* detector with some additional equipment, the verification of the redshift mechanism may be performed in parallel with the main task or during a calibration stage of the detector. The positive expected result of such the experiment would mean also that the universe does not expand.

It seems that to open minds for the broader perception of possible manifestations of quantum gravity and ways to its future theory, we should doubt in some commonly accepted things. The very bright example is the claimed existence of dark energy that is unnecessary in the considered model. If redshifts of remote objects have the local quantum nature, the expansion of the universe becomes not necessary, and some observable effects may be interpreted as the long-awaited exhibition of quantum gravity but in the absolutely unexpected scale of energies $\sim 10^{-3}$ eV. This scale may move us much closer to the understanding of the existing chasm between general relativity and quantum mechanics. And, perhaps, it can give us chances to construct if not a bridge between them, then a new common base for both.

References

[1] Nicolai, H. Gravity's quantum side. [https://cerncourier.com/a/gravitys-quantum-side/].

[2] Ivanov, M.A. The system of equations describing 4 generations with the symmetry group $SU(3)_C \times SU(2)_L \times U(1)$ (in Russian). Deposited in VINITY 19.12.1988 as VINITI No 8842-B88; in English: [https://vixra.org/pdf/2006.0185v3.pdf].

[3] Ivanov, M.A. Primary postulates of the standard model as consequences of the composite nature of the fundamental fermions. *Nuovo Cimento* 1992, *105A,* 77. [hep-th/0207210].

[4] Ivanov, M.A. Possible manifestations of the graviton background. *Gen.Rel.Grav.* 2001, *33*, 479-490; Erratum-ibid. 2003, *35*, 939-940. [arXiv:astro-ph/0005084v2].

[5] Ivanov, M.A. "Gravitons as super-strong interacting particles, and low-energy quantum gravity". In *Focus on Quantum Gravity Re-*

search, 89-120, edited by D.C. Moore, NY: Nova Science, 2006. [arXiv:hep-th/0506189v3].

[6] Ivanov, M.A. Selected papers on low-energy quantum gravity. [https://vixra.org/pdf/1110.0042v2.pdf].

[7] Ivanov, M.A. Low-energy quantum gravity and cosmology without dark energy. *Advances in Astrophysics* 2019, 4, No. 1, 1-6.

[8] Ivanov, M.A. Lorentz symmetry violation due to interactions of photons with the graviton background. [arXiv:0907.1032v2 [physics.gen-ph]].

[9] Ivanov, M.A., Narkevich, A.S., and Shenetz, P.S. Modified dynamics due to forehead collisions of bodies with gravitons: Numerical modeling. [http://vixra.org/pdf/1706.0427v1.pdf].

[10] Ivanov, M.A. Modified dynamics of massive bodies in the graviton background. [https://vixra.org/pdf/1907.0257v2.pdf].

[11] Ivanov, M.A. Galaxy number counts in a presence of the graviton background. [arXiv:astro-ph/0606223v3].

[12] Cunha, J. V., Lima, J. A. S., N. Pires. Deflationary cosmology: $\Lambda(t)$ Observational expressions. *A&A* 2002, *390*, 809-815.

[13] Loh, E.D. and Spillar, E.J. A Measurement of the Mass Density of the Universe. *ApJ* 1986, *307*, L1.

[14] Schechter, P.L. An analytic expression for the luminosity function for galaxies. *ApJ* 1976, *203*, 297-306.

[15] Yasuda, N. et al. Galaxy number counts from the sloan digital sky survey commissioning data. *AJ* 2001, *122*, 1104-1124.

[16] Ivanov, M.A. Cosmological consequences of the model of low-energy quantum gravity. Proc. Int. Conf. "Cosmol- ogy on Small Scales 2016", M. Krizek and Yu. Dumin (Eds.), Institute of Mathematics CAS, Prague, pp 179-198. [http://http://css2016.math.cas.cz/proceedingsCSS2016.pdf].

[17] Riess, A.G., et al. Type Ia Supernova Discoveries at z¿1 From the Hubble Space Telescope: Evidence for Past Deceleration and Constraints on Dark Energy Evolution. *ApJ,* 2004, *607,* 665-687. [astro-ph/0402512].

[18] Suzuki, N. et al. The Hubble Space Telescope Cluster Supernova Survey: V. Improving the Dark Energy Constraints Above $z > 1$ and Building an Early-Type-Hosted Supernova Sample. *ApJ* 2012, *746*, 85. [arXiv:1105.3470v1 [astro-ph.CO]].

[19] Betoule, M., et al. Improved cosmological constraints from a joint analysis of the SDSS-II and SNLS supernova samples. *A&A* 2014, *568*, A22. [arXiv:1401.4064v2 [astro-ph.CO]].

[20] Wei, H. Observational Constraints on Cosmological Models with the Updated Long Gamma-Ray Bursts. *JCAP* 2010, *08*. [arXiv:1004.4951v3 [astro-ph.CO]].

[21] Lin, H.-N., Li, X., and Chang, Z. Effect of GRB spectra on the empirical luminosity correlations and the GRB Hubble diagram. *MNRAS* 2016, *459*, 2501-2512. [arXiv:1604.02285 [astro-ph.HE]].

[22] Risaliti, G., and Lusso, E. A Hubble Diagram for Quasars. *ApJ,* 2015, *815,* 33; [arXiv:1505.07118 [astro-ph.CO]].

[23] Lopez-Corredoira, M., Melia, F., Lusso, E., and Risaliti, G. Cosmological test with the QSO Hubble diagram. *International Journal of Modern Physics D* 2017, *25*, No. 05, id. 1650060. [arXiv:1602.06743 [astro-ph.CO]].

[24] Farooq, O., and Ratra, B. Hubble parameter measurement constraints on the cosmological deceleration-acceleration transition redshift. *ApJ letters* 2013, *766*, 1, L7. [arXiv:1301.5243].

[25] Riess, A. G., et al. A 3% Solution: Determination of the Hubble Constant with the Hubble Space Telescope and Wide Field Camera 3. *ApJ* 2011, *730*, 119.

[26] Moresco, M. Raising the bar: new constraints on the Hubble parameter with cosmic chronometers at $z \simeq 2$. *MNRAS Letters*, 2015 *450*, Issue 1, L16-L20. [arXiv:1503.01116v1 [astro-ph.CO]].

[27] Alcock, C. and Paczynski, B. An evolution free test for non-zero cosmological constant. *Nature* 1979, *281*, 358-359.

[28] Melia, F., and Lopez-Corredoira, M. *International Journal of Modern Physics D* 2017, *26*, Issue 6, id. 1750055-265. [arXiv:1503.05052v1 [astro-ph.CO]].

[29] Anderson, L., et al. The clustering of galaxies in the SDSS-III Baryon Oscillation Spectroscopic Survey: baryon acoustic oscillations in the Data Releases 10 and 11 Galaxy samples. *MNRAS* 2014, *441*, 24-62.

[30] Delubac, T., et al. Baryon acoustic oscillations in the Lyα forest of BOSS DR11 quasars. *A&A* 2015, *574*, A59.

[31] Wu, Junfei, et al. Progress in Precise Measurements of the Gravitational Constant. *Annalen Phys.* 2019, *531*, 5, 1900013.

[32] Melia, F., and Yennapureddy, M.K. Model selection using cosmic chronometers with Gaussian Processes. *JCAP* 2018, *2018*, 02, 034. [arXiv:1802.02255v2 [astro-ph.CO]].

[33] Lauer,T.R., et al. New Horizons Observations of the Cosmic Optical Background. [arXiv:2011.03052v2 [astro-ph.GA]].